



LARGE-SCALE EXPERIMENT OF A NEW HOLLOW-CORE TIMBER SLAB SYSTEM

Cristóbal Tapia¹, Kai Simon², Aaron Münzer³, Lisa Stimpfle⁴, Simon Aicher⁵

ABSTRACT: A new concept of a hollow-core timber slab was experimentally tested under punching loading conditions. The concept consists of CLT plates serving as flanges and a set of GLT elements acting as webs, with a solid LVL element reinforcing the point-supported region. Further, a beech LVL is applied as tensile reinforcement against negative moments in the support region. The specimen, measuring 3.2 m in length and 2.2 m in width, was initially subjected to a cyclic loading regime, totaling 2.8 million cycles at different load levels, of which 1.8 million cycles were performed at about 58 % of the specimen's ultimate capacity and a stress ratio of $R = 0.79$. Subsequently, quasi-static loading was applied until failure. The results indicate only marginal damage after the 2.8 million cycles, evidenced by a decrease in global stiffness of the system of approximately 2 %. Ultimate capacity was reached at $F = 1.6$ MN, with failure initiating at one of the GLT web elements, causing a redistribution of load to adjacent elements, leading to tension failure in the beech LVL reinforcement. A fatigue analysis according to EC 5-2, assuming shear failure, showed no risk of fatigue failure, which is likely due to the relatively high degree of redundancy in the system.

KEYWORDS: multi-storey buildings, hollow-core slab, fatigue, point-support, CLT

1 – INTRODUCTION

The timber building industry has been increasingly adopting the construction of high-rise buildings, as made evident by the steadily increasing number of such projects [13] and related scientific output on diverse associated aspects, such as connections and structural systems. Major driving forces for this development are the needed densification of cities, i.e. a more efficient use of urban space, together with the general objective to reduce the CO₂ footprint associated to the building sector. The densification of cities is needed to overcome the increasing housing strain seen currently in large cities, and building vertically is a space-efficient solution to this problem.

The current trend of multi-storey timber buildings does not follow a single specific pattern regarding the structural system or the type of elements employed, presenting a varied mix of structural systems such as timber frames [8], point-supported slabs with concrete core [6] or panel systems. A comprehensive analysis of recent projects of multi-storey timber buildings was compiled and analyzed recently by Svatoš-Ražnjević et al. [13], revealing that despite the differences in structural systems, a common characteristic to most of the analyzed buildings was the reliance on rectilinear grid-based structures. This characteristic constitutes a constraint on the design flexibility of internal spaces, as argued e.g. in [11], as the spacing of the

grid determines the possible internal room configurations. A simple solution to increase the grid spacing is to consider a post-and-beam system, where beams are spanned between columns to support plate elements. However, this comes at the cost of losing a flat ceiling surface, undermining the reconfigurability potential of the spaces.

For systems based on point-supported plates, such as in [6], the grid spacing is limited by the size of the used cross-laminated timber plates (CLT), which depends on both manufacturing and transportation constraints. In general, this leaves maximum plate widths of about 3 m and lengths of about 6 m. In order to overcome the limitation on the grid spacing—especially in the secondary direction of the CLT—stiff and reliable edge connections are required in order to fully activate the biaxial behavior of the plates, together with concepts for the reinforcement of point-supported regions within the slab.

Point-supported slabs in timber structures generally present a challenge due to the high concentration of shear forces in the supported region, requiring special detailing concepts. Additionally, if the column is placed in the inner region of the slab, the localized negative moment will induce tensile stresses in the upper layers of the CLT plate, which can become critical due to the presence of openings for the vertical transfer of loads between columns, as stress concentrations will occur (see e.g. [10]). The relevance of this type of connection has led to the development of dif-

¹ Cristóbal Tapia, Materials Testing Institute (MPA), University of Stuttgart, Stuttgart, Germany, Email: cristobal.tapia@mpa.uni-stuttgart.de

² Kai Simon, Materials Testing Institute (MPA), University of Stuttgart, Stuttgart, Germany, Email: kai.simon@mpa.uni-stuttgart.de

³ Aaron Münzer, Materials Testing Institute (MPA), University of Stuttgart, Stuttgart, Germany, Email: aaron.muenzer@mpa.uni-stuttgart.de

⁴ Lisa Stimpfle, Materials Testing Institute (MPA), University of Stuttgart, Stuttgart, Germany, Email: lisa.stimpfle@mpa.uni-stuttgart.de

⁵ Simon Aicher, Materials Testing Institute (MPA), University of Stuttgart, Stuttgart, Germany, Email: simon.aicher@mpa.uni-stuttgart.de

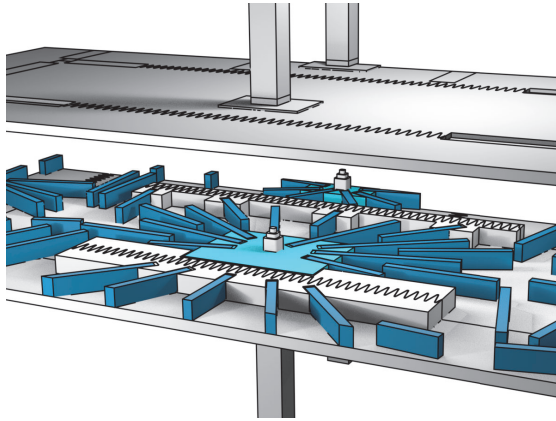


Figure 1: General concept of the investigated hollow-core timber slab system. Possible edge connections close to the crown area are shown in the form of large-scale finger-joints.

ferent approaches to designing such details. For example, specially developed steel elements for the reinforcement of the point-supported region and vertical transfer of loads are presented in [5, 6], while a purely timber-based solution for this situation was presented in [14, 15]. The reinforcement of negative-moment-induced tensile stresses by means of glued-on plates was studied in [10], which was also covered in the design presented in [14].

Stiff edge connections for CLT plates have been an important research topic in recent years, with several new concepts and products being introduced, evidencing the large potential for the practical application in building projects [1, 7, 12, 16, 18]. Although these are valid solutions, the efficiency of the system in terms of material use will decline for long spans, as the required cross-sectional depths needed to comply with the serviceability limit state increase with the span.

To overcome this issue, a new hollow core slab concept was developed in [11] and initial experimental results were presented in [17]. The slab system consists of two outer CLT elements acting as *flanges*, and a set of discretely distributed *web* elements made of glued laminated timber (GLT), as shown in Fig. 1. The region in contact with the supporting column is reinforced by means of a solid laminated veneer lumber (LVL) block (here termed *crown*) to handle the high shear forces. The GLT web elements in the periphery of the crown are oriented in a radial pattern and glued to the crown to transfer the shear forces.

In a previous investigation of this new system, reported in [17], the focus was laid on the study of the connection between GLT web elements and the LVL crown by means of an adhesive bonding. Simplified, uniaxial experiments on isolated crown-web components with varying bonding surfaces were made and compared with a detailed 3D finite element (FE) model, where the distributions of shear stress on the bonding area was assessed. Two different adhesives were tested, these being a melamine-urea-formaldehyde (MUF) and a two component epoxy. The results showed that an efficient bonding is achieved when the web element

is fully embedded, i.e. glued, into the LVL crown by applying the two-component epoxy adhesive on all vertical surfaces.

Additional experiments were later realized to assess the behavior of the web elements glued at an angle with respect to the LVL crown [9]. The different configurations were tested in three-point bending and gradually resembled the *real* situation at the point-supported region of the slab by firstly including the top and bottom CLT layers, and finally testing a simplified version of the connection detail with four web elements connected to the crown at an angle with respect to the bending axis. The results were positive, thus clearing the path for the testing of the full-sized connection detail reported below.

This paper focuses on the experiment of a full-sized connection detail of the newly-developed hollow-core timber slab system. Firstly, the system will be described in detail, followed by the definition of the experimental setup and loading protocol. Thereafter, the used material is characterized and the manufacturing process for the specimen is described. The results are then presented, followed by a discussion and finalizing with some concluding remarks.

The concept was developed within the Cluster of Excellence “Integrative Computational Design for Construction and Architecture” (IntCDC) at the University of Stuttgart and is intended to be applied in the design of the new “Large-Scale Construction Robotics Laboratory” (LCRL) in Stuttgart. The presented experiment considers some of the specific requirements of this building.

2 – HOLLOW-CORE SLAB SYSTEM

The developed system follows the principle of a hollow-core slab or box girder, where CLT plates act as the outer flanges, and short GLT beams serve as web elements. The web elements are distributed throughout the slab, aligned with the local principal bending direction at each position. Directly above the column (point support) the system considers a series of different elements and features, as shown in Fig. 2.

Firstly, a hole is considered throughout the depth of the slab system to allow for the transfer of vertical loads from column to column by means of a hardwood pin element (see also [15]). The region of the lower CLT plate surrounding the hole, and directly in contact with the column below, is reinforced with a small beech LVL element, here termed *transfer plug*. Directly above, between both CLT plates, a large softwood LVL block is located (here termed *crown*). This has the purpose to provide enough material to resist the expected high shear stresses in this region. The web elements on the periphery of the LVL crown are oriented radially with respect to the center of the hole, and are embedded into the crown in pre-milled cavities (see Fig. 2). The embedding is secured by means of a two-component, gap-filling epoxy adhesive. Both crown and web elements are glued to both CLT plates by means of screw-press gluing.

The top CLT plate is reinforced with a beech LVL plate as shown in Fig. 2. This plate is assembled of two LVL plates

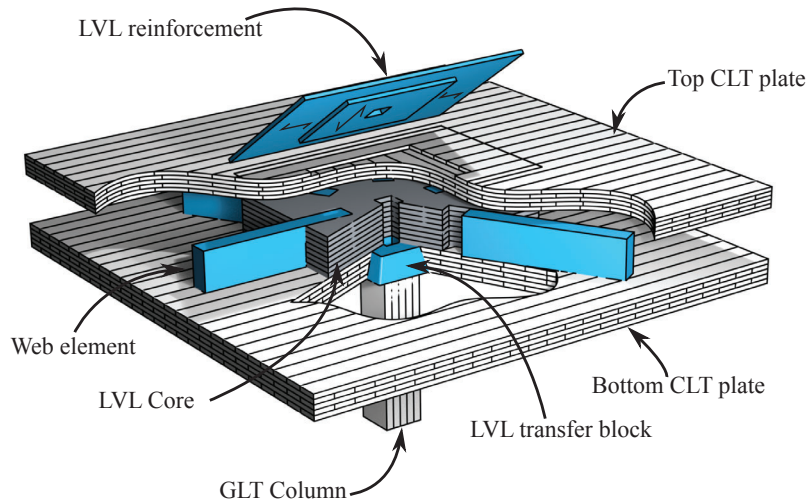


Figure 2: Concept point-supported hollow-core plate system

oriented perpendicular to each other. The reinforcement plate is glued into a cavity on the top CLT plate, such that the lower layer is glued onto the second layer of the CLT, thus reinforcing the secondary direction. Analogously, the top layer of the LVL plate is glued onto the first layer of the CLT, thus reinforcing in the principal direction of the plate. The LVL reinforcement is screw-press glued using an phenol-resorcinol-formaldehyde (PRF) adhesive.

3 – MATERIALS AND METHODS

3.1 EXPERIMENTAL CONFIGURATION

The experiment is designed to investigate the punching behavior of the studied slab system. To this end, a slab section of 3.3 m in length and 2.3 m in width is considered. The LVL crown element, with dimensions 1960 mm × 1510 mm, is positioned at the center, featuring twelve radially oriented web elements with cross-sections of 200 mm × 100 mm em-

bedded approximately 300 mm into the crown (see Fig. 3b). The length of each GLT beam extends to the perimeter of the slab.

A rectangular hole, with dimensions 232 mm × 232 mm, is included at the slab's center to account for the intended—though not part of this experiment—vertical load transfer between columns. Additionally, a smaller hole is included to address a specific requirement of the LCRL building, where such openings are necessary for rainwater pipe pass-throughs.

The complete slab is inverted and line-supported by steel roller bearings of diameter 70 mm, which are positioned atop steel beams along each of the four edges (see Fig. 3a). Lateral stoppers are installed on each side to prevent potential excessive lateral displacements during initial cyclic loading, as shown in Fig. 4. The load is applied at the plate's center, directly on a short column segment made

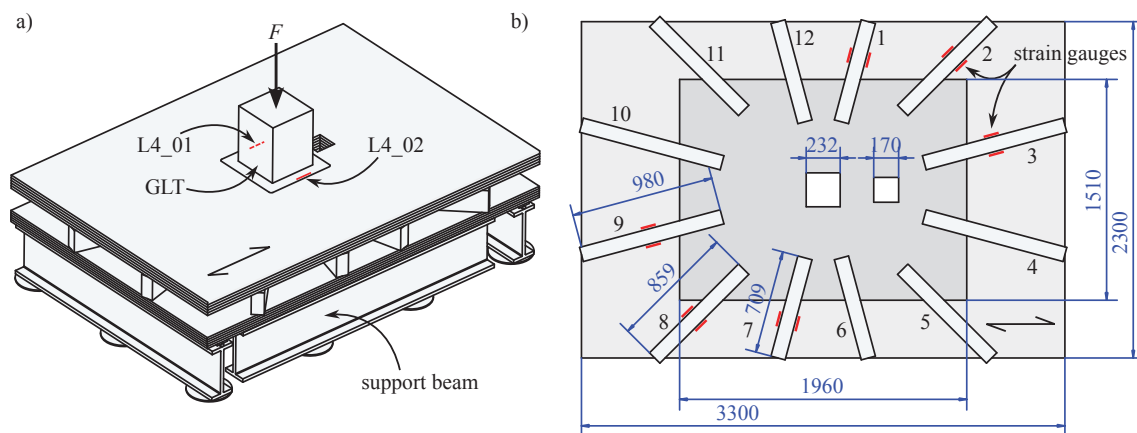


Figure 3: Geometry, dimensions and position of measuring points for the experimental setup of the developed hollow-core slab system; (a) isometric view of the set-up, (b) top view of the specimen without the top-most CLT plate and location of three-axial strain gauges in web elements (dimensions in mm)

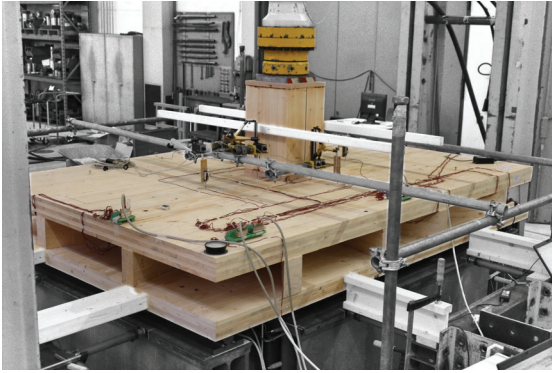


Figure 4: Realized experimental set-up for the punching test and support structure for the positioning of instrumentation

Table 1: Load stages used during the cycling loading of the specimen

Stage	mean [kN]	$F_{\min}-F_{\max}$ [kN]	amplitude [kN]	R^* [-]	N [-]
1	225	100–350	250	0.29	250 000
2	400	300–500	200	0.60	240 000
3	550	450–650	200	0.70	260 000
4	700	600–800	200	0.75	220 000
5	850	750–950	200	0.79	1 780 000

$$^* R = \sigma_{\min}/\sigma_{\max}$$

from GLT with a cross-section of 400 mm × 400 mm. The loading cylinder had a maximum nominal load capacity of 2 MN.

3.2 LOADING PROTOCOL

The experiment consisted of three consecutive loading stages, performed in the following sequence:

1. First, the specimen was loaded quasi-statically three times consecutively up to a load of 400 kN. For each loading ramp, the load was maintained for one minute upon reaching the target load, after which the specimen was unloaded.
2. Following this, a cyclic loading protocol with a frequency of 0.5 Hz was performed. The load amplitude and range were varied according to the information presented in Table 1. In total, approximately 2.8 million cycles were conducted between November 2023 and February 2024.
3. Finally, three quasi-static loading ramps were performed, with the first two loading up to 1 MN, and the third until global failure occurred.

The experiment took place in an acclimatized laboratory at the Materials Testing Institute of the University of Stuttgart, with a mean measured temperature and relative humidity of approximately 20 °C and 50 %, respectively. The cyclic testing was interrupted between mid-December and mid-January for about 36 days due to holidays. This

was at the end of the third loading stage according to Table 1.

3.3 INSTRUMENTATION

To enable a detailed understanding of the mechanical behavior of the specimen during the different loading stages, a variety of sensors was employed. These sensors included strain gauges, linear variable displacement transducers (LVDTs) and fiber-optic cables for strain measurement. In addition, the room temperature and relative humidity were continuously recorded throughout the entire experiment.

Uniaxial strain gauges were applied on both CLT plates, on the tension reinforcement, and on the LVL crown element (see Fig. 3a for a subset of the applied strain gauges). Two strain gauges (L4_05 and L4_06) were placed close to one of the corners of the central opening, in the region where stress concentrations were expected. Three-axial strain gauges were installed on both sides of six web elements—numbered 1, 2, 3, 7, 8, and 9—as shown in Fig. 3b. This allowed for measurement of shear strains and determination of the exact moment of failure for each component. In total, 27 uniaxial and twelve three-axial strain gauges were used.

A total of twelve LVDTs were used to measure vertical displacements on the upper CLT plate. Four LVDTs were positioned around the periphery of the central GLT element (loading point), at a distance of 50 mm from each side. Four additional LVDTs were placed at a distance of 535 mm from each side of the central GLT element.

Finally, four fiber-optic cables were glued onto the CLT plates, tension reinforcement, and LVL crown. However, these data are not further analyzed in this paper.

Due to the relatively large number of sensors and the consequent large quantity of associated measuring channels, two distinct measuring amplifiers were employed. One of these devices recorded continuously throughout all loading stages, whereas the other amplifier was disconnected for an extended interval during cyclic loading, as it was required for a different experiment. This disconnection led to information gaps for the sensors connected to that amplifier. During the quasi-static loading tests, both amplifiers were continuously connected.

3.4 MATERIALS

For the CLT plates, two different cross-sections each with 5 layers were used, with thicknesses of 100 mm (top plate) and 120 mm (bottom plate). The plates were manufactured according to the ETA-10/0241 [4]. The moisture content (MC) was measured with a resistometer at different locations prior to assembly, giving an average of 9.9 %.

The GLT elements correspond to the GL24 class with a cross-section of 100 mm × 200 mm, and had an average 11.6 %. The softwood LVL block used for the crown element is composed of six layers of 33 mm thick unidirectional spruce LVL, stacked on top of each other. The layers are oriented perpendicular to each other in an alternating pattern.

For both the transfer plug and the tension reinforcement, beech LVL (BauBuche) [2] was used. The tension reinforce-

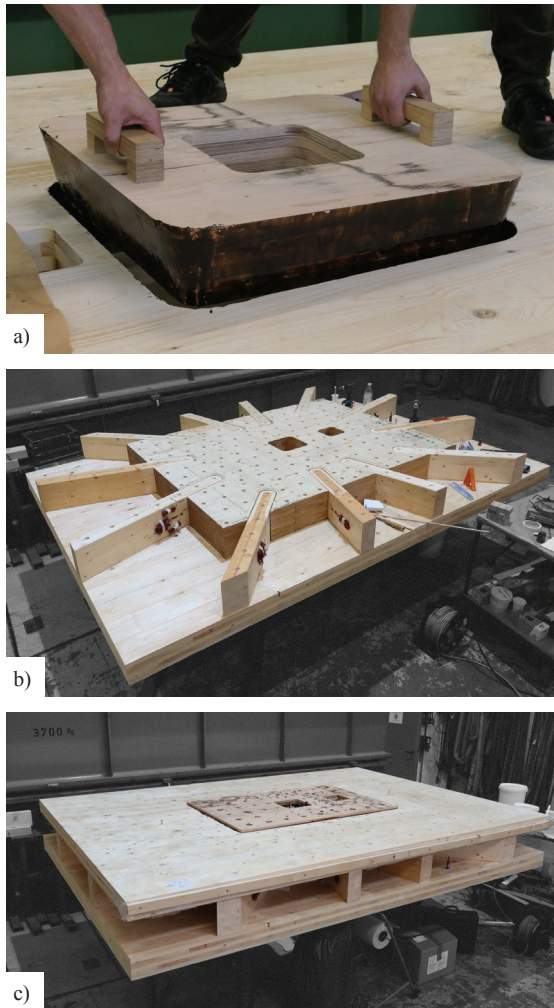


Figure 5: Different stages of the manufacture process: (a) gluing of the plug element in the compression region; (b) screw-press gluing of crown and web elements; (c) application of upper CLT plate with tension reinforcement.

ment is composed of two layers of 20 mm each, oriented perpendicular to each other (see Fig. 2). The transfer plate was assembled from six 20 mm layers, oriented perpendicular to each other. Both elements had an average moisture content of 10.8 % before assembly.

4 – MANUFACTURE OF THE SPECIMEN

The individual components were milled at Züblin Timber GmbH, Aichach, Germany, and then delivered to the Materials Testing Institute at the University of Stuttgart, where the specimen was assembled. The assembly process consisted of the sequential attachment of the following components: (i) transfer plug, (ii) crown element, (iii) web elements, (iv) tension plate, and finally (v) top CLT plate.

The transfer plug was glued into the bottom CLT plate using a phenol-resorcinol-formaldehyde (PRF) adhesive, as shown in Fig. 5a, and was held in place during adhesive

curing by means of screw clamps. Subsequently, the crown element was attached to the bottom CLT plate by screw-press gluing with an melamine-urea-formaldehyde (MUF) adhesive (800 g/m²), following prior sanding of the surfaces of both elements. Attention was paid to maintaining a clean perimeter—free of adhesive excess—for embedding the web elements.

Next, the web elements were screw-press glued to the bottom CLT plate using the same MUF adhesive as above (700 g/m²), as illustrated in Fig. 5b. The 5 mm gap between the web elements and the crown was first sealed with adhesive tape as preparation for adhesive injection. A gap-filling, two-component epoxy adhesive was then injected into the gap through inclined, pre-drilled holes from the top surface of the crown, filling the gap progressively from the bottom upwards.

Meanwhile, the first layer of the beech LVL tension reinforcement was screw-press glued into the cavity of the top CLT plate, followed by the second layer. A PRF adhesive was used for both reinforcement layers. Finally, the top CLT plate was glued onto the crown and web elements using screw-press gluing (see Fig. 5c).

The entire assembly process took approximately three days. A major bottleneck was the gluing of the transfer plug, as it required waiting a full day before proceeding with the crown and web elements. The gluing operations for the different components on the top and bottom CLT plates were carried out in parallel, which helped to accelerate the overall process. Generally, the concept appears to be suitable for serial production, particularly when considering the number of elements needed for an entire building. Additionally, the use of robotic fabrication systems seems applicable to the assembly steps.

5 – RESULTS

5.1 CYCLIC LOADING

The data from each sensor were averaged over one-minute intervals to analyze the trend across the number of cycles. Figure 6a shows the averaged strain measured by the sensors located on the outer surfaces of the upper (compression) and lower (tension) CLT plates. The selected strain gauges are oriented parallel to both the specimen's main axis and the grain direction. The different loading stages are indicated by vertical dashed lines, and the respective stage numbers are annotated in each region (cf. Table 1).

Figure 6a shows a steady increase in the measured strains. A discontinuity occurs at the interface between loading stages due to differences in the applied load. During the final stage, at a load of 850 ± 100 kN, all curves except one show a similar trend, with no evident signs of major damage. For the measuring point L1_01, located on the LVL tension reinforcement, next to the large hole, a slow decrease in strain starting at around 1.3×10^6 cycles is visible. As none of the other strain gauges show a significant deviation from their respective trends, the observed behavior at L1_01 can likely be attributed to local damage or local softening. It is possible that this relates to the bond line between the beech

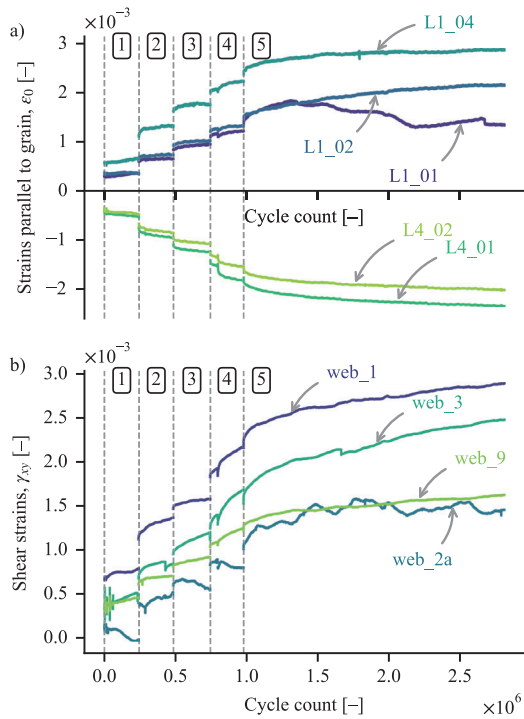


Figure 6: Evolution of strains with the number of cycles for subset of strain gauges. Vertical dashed lines mark the regions corresponding to the different load levels according to Table 1.

LVL and the CLT plate; however, this cannot be stated with certainty.

Figure 6b presents the results of the same aggregation procedure described above, now applied to shear strains measured on the web elements. Additionally, the measurements from sides *a* and *b* of each web were averaged, except for web 2, whose side *b* presented measurement errors; thus, only side *a* results are shown—explaining why this curve is less smooth than the others. Measurement data for webs 7 and 8 were incomplete (see above) and were therefore omitted from Figure 6b.

The shear strain evolution shown in Fig. 6b generally follows a similar behavior as discussed above (Fig. 6a) for normal strains. A slight drop in strain occurs for web 3 around 1.5×10^6 cycles, however, this does not significantly affect the general trend. Based on these curves, it can be concluded that no major damage occurred within the web elements or the bond lines between CLT plates and web beams during cyclic loading.

5.2 INFLUENCE OF CYCLIC LOADING ON STIFFNESS

The load-displacement curves from the quasi-static tests before and after cyclic loading are shown in Fig. 7. The displacement corresponds to the average reading of the four LVDTs surrounding the load application point. A slight stiffness reduction of approximately 2% can be observed,

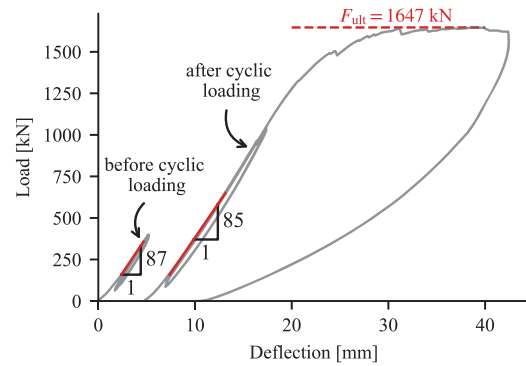


Figure 7: Comparison of the stiffness of the system during quasi-static loading before and after the cyclic loading regime.

which is consistent with the results presented in Figs. 6a and 6b, where no significant damage was detected due to the cycling loading.

5.3 BEHAVIOR AT ULTIMATE CAPACITY

The complete load-displacement curve for the experiment is shown in Fig. 7. Linear behavior is observed up to about 1300 kN, after which the curve begins to flatten, eventually reaching a maximum load of $F_{\max} = 1647$ kN. The experiment was stopped at approximately 35 mm deflection (note that the curve in Fig. 7 is shifted to the right for improved clarity). Thus, it is evident that significant damage occurs at around 1.32 MN, leading to internal stress redistributions that are analyzed in detail below.

Figures 8a and b present the shear strains measured on webs 1, 2, 3, 7, 8, and 9, along with the computed shear stresses, for the first and final loading cycles of the ultimate capacity test, respectively. Figure 8a shows some damage occurring on web 8 at a load level of about $F = 1000$ kN. However, this damage appears to have a negligible influence at the global scale, as supported by the load-displacement curve in Fig. 7. It is worth noting that, due to the nearly symmetric geometry, similar behavior is expected between webs 1 and 7, 2 and 8, and 3 and 9. However, this symmetry is not reflected in the data. To some extent, these deviations may be attributed to minor eccentricities in the test set-up or some damage introduced during the cyclic loading. However, similar discrepancies were also observed in measurements performed prior to cyclic loading (not shown here).

Figure 8b shows the measured shear strains in the web elements until the maximum capacity is reached. Linear behavior is observed for each curve until approximately $F = 1300$ kN, at which point significant damage occurs in web 7, which can be attributed to a shear failure in the bond line, as shown in Fig. 9b. The corresponding shear stress is about 1.7 MPa, well below the characteristic shear strength of GLT of $f_{v,k} = 3.5$ MPa. This corresponds also to the point at which the global load-displacement curve becomes nonlinear (see Fig. 7). The load then redistributes to the neighboring web elements 8 and 9, indicated by an increase

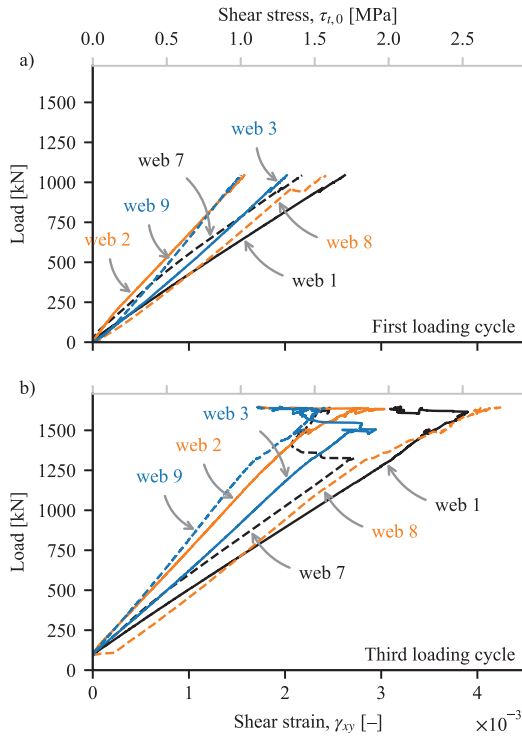


Figure 8: Shear strains during the first and third (ultimate capacity) loading cycles. Results correspond to the average of the measurements at both sides of each web.

in the measured strains. Further damage subsequently occurs in web 3 at approximately $F = 1500$ kN, followed by a corresponding increase in strains in the adjacent web 2. The load continues to increase thereafter until major failure occurs in webs 1, 2, and 3. No further load increase is possible beyond this point.

Figure 10 shows the strains measured at selected points on the beech LVL tension reinforcement and the computed stresses assuming $E_0 = 16800$ MPa (see Fig. 9c). This region is of particular interest, as it is subjected to high tensile stresses and therefore represents a potential location for damage initiation. The behavior is linear until about $F = 1200$ kN, at which load level position L1_05 exhibits some nonlinear behavior. Position L1_04, located at a distance of 10 mm from L1_05, exhibits no such marked nonlinearity. Thus, the nonlinear behavior of L1_05 seems highly localized.

At a load of about $F = 1300$ kN, coincident with the damage in web 7 (see Fig. 8b), clear nonlinearities are observed at positions L1_01, L1_02, and L1_06. With further increase in the load, damage continues to propagate until a complete failure is observed at the ultimate load of $F = 1.6$ MN. Positions L1_04 and L1_05 indicate considerable damage in the beech LVL plate shortly before global failure, at a stress level of approximately 75 MPa, which is above the characteristic value for the material of

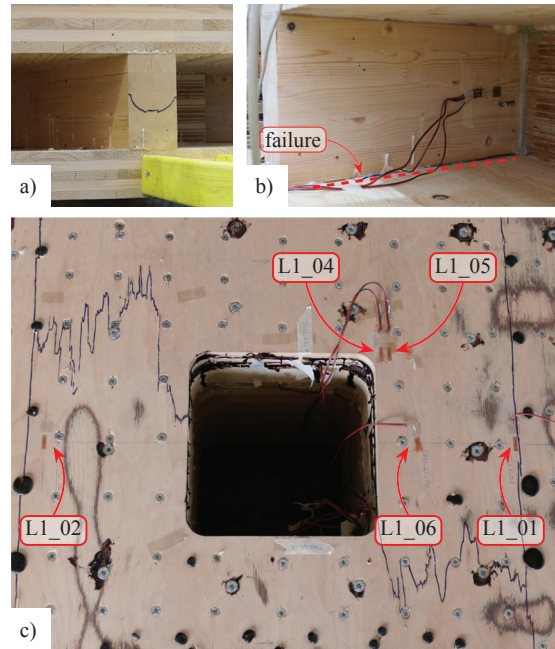


Figure 9: Damage in the specimen after ultimate capacity. (a) shear failure in web 4; (b) shear failure on the bond line of web 7; (c) tensile failure in the tension reinforcement

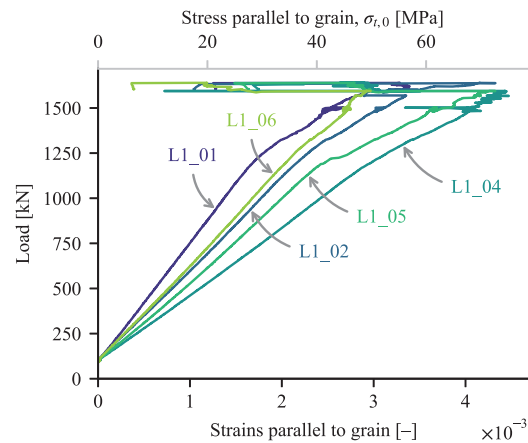


Figure 10: Strains parallel to the fiber and computed stresses on the beech LVL tension plate during the loading until global failure

$f_{t,0} = 60$ MPa. This means that this tension failure was probably responsible for the global failure of the specimen. The damage in the tension region on the reinforcement plate is evident in Fig. 9c.

According to this analysis, the failure most likely initiated at web 7 (Fig. 9b), subsequently causing a load redistribution that eventually led to the failure of neighboring elements (Fig. 9a) and, ultimately, the tension reinforcement region (Fig. 9c), leading to global failure of the specimen. This load redistribution indicates a high degree of redun-

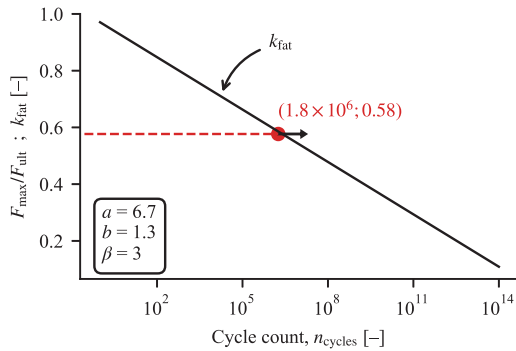


Figure 11: Comparison of k_{fat} according to EN 1995-2 [3] and the result from the experimental cyclic loading

dancy within the system, enabling further load increases even after the failure of some elements.

5.4 CONSIDERATION OF FATIGUE ACCORDING TO EUROCODE 5-2

Although only one specimen was tested, and cyclic loading was stopped before fatigue failure occurred, an analysis based on EN 1995-2 [3] can still be performed. Specifically, the experimental result can be presented along with the fatigue reduction factor k_{fat} corresponding to the relevant failure mode, which is computed as a function of the number of cycles n_{cycles} as follows:

$$k_{fat} = 1 - \frac{1 - R}{a(b - R)} \cdot \log(\beta \cdot n_{cycles}), \quad (1)$$

with parameters a and b according to Fig. 11, which assumes shear failure [3]—as experimentally observed—and considers damage with substantial consequences via parameter $\beta = 3$. The value of the stress ratio is $R = \sigma_{min}/\sigma_{max} = 0.79$, applied in loading stage 5. For evaluating the experimental result, only the cycles in stage 5 (the final loading stage; see Table 1) were considered, thus, $n_{cycles} = 1.8 \times 10^6$. This results in $k_{fat} = 0.58$ after applying (1).

Figure 11 shows a comparison between the single experimental data point $F_{max}/F_{ult} = 0.58$ and the k_{fat} reduction factor. It can be observed that the experimental result lies—by pure chance—almost exactly on the k_{fat} curve. Since no signs of considerable damage were observed during cyclic loading at load level $F_{max}/F_{ult} = 0.58$, it can be assumed that the specimen likely presents a much higher resistance under fatigue loading. Consequently, the actual k_{fat} reduction factor for the specimen is certainly higher than the one computed with the parameters provided in EN 1995-2 [3].

6 – DISCUSSION

The slab system investigated in this study was developed specifically for cases requiring long spans, flexible positioning of columns, and reconfigurable internal spaces. Considering these requirements, along with the objective

of creating a concept based entirely on timber elements, resulted in the need for precise milling and assembly of multiple components. As such, it is evident that the presented system cannot compete with typical multi-storey building systems in terms of costs and manufacturing effort. Nevertheless, the presented concept was conceived with a high degree of automation in mind, allowing current robotic manufacturing technologies to be leveraged for achieving high economic efficiency. The development and application of digital fabrication technologies is a key research topic within the IntCDC cluster, and ongoing research aims at further lowering costs, thus improving the economic viability.

The experiment demonstrated highly redundant behavior in the point-supported region of the slab system, enabling load redistribution to neighboring elements. The varying orientation of the web elements relative to the fiber direction of the CLT layer to which they are glued did not create problems in general. However, large fiber deviation at web element 7—oriented nearly perpendicular to the fiber direction of the CLT—was responsible for initiating global failure, exhibiting clear rolling shear failure at the bond line.

Although the maximum capacity achieved meets the requirements for the intended use, improvements could be implemented to improve the performance of web elements attached at angles close to perpendicular relative to the fiber direction. One possibility involves gluing these webs to the next (perpendicular) CLT layers by milling cavities matching the geometry of the web elements, with the objective of reducing the angle to the fiber. This measure would, of course, increase manufacturing effort. However, it would create a significantly more robust bond between the web elements and the CLT plates.

7 – CONCLUSIONS AND OUTLOOK

A full-scale specimen representing a novel concept for a point-supported hollow-core slab system was experimentally tested under a punching load setup. The specimen had dimensions of 3.3 m in length and 2.3 m in width, and included twelve radially oriented GLT web elements. The experiment aimed to investigate two aspects of the system: (i) the effect of fatigue loading on the overall stiffness of the system and damage accumulation in its various components, and (ii) the failure mode of the system under quasi-static loading at ultimate capacity. Based on the analysis of experimental results, the following conclusions can be drawn:

1. Cyclic loading at 58 % of maximum capacity with a stress ratio $R = 0.79$ did not cause significant damage up to at least 1.8×10^6 cycles;
2. A total of 2.8×10^6 loading cycles at varying load levels only reduced the stiffness of the system by approximately 2 %;
3. Global failure of the specimen was initiated by shear failure in one of the GLT web elements, leading to

load redistribution among the remaining components and eventually triggering overall collapse due to a tension failure at the beech LVL reinforcement plate;

4. A simplified analysis based on EN 1995-2 [3] indicates that the studied specimen should not suffer from fatigue-related issues.

The presented slab system is planned to be utilized in the new Large-Scale Construction Robotics Laboratory (LCRL) of the Cluster of Excellence “Integrative Computational Design for Construction and Architecture” (IntCDC) at the University of Stuttgart. The presented results contribute to ensuring the safety and performance of this building.

The experimental results will be further analyzed and compared with a detailed finite element model. This will allow for a better understanding of the interactions between components under different loading conditions, thereby assisting in the design of such elements.

ACKNOWLEDGEMENTS

The presented ongoing research is supported by the Deutsche Forschungsgemeinschaft (DFG, German Research Foundation) under Germany’s Excellence Strategy – EXC 2120/1 – 390831618. The authors would like to thank Mr. Thomas Mantzel from the company Züblin Timber GmbH for his support with the milling of the needed components.

REFERENCES

- [1] J. Asselstine, F. Lam, and C. Zhang. “New edge connection technology for cross laminated timber (CLT) floor slabs promoting two-way action.” In: *Engineering Structures* 233 (2021), p. 111777. DOI: 10.1016/j.engstruct.2020.111777.
- [2] DOP PM-020-2024. *Laminated veneer lumber made from beech – Laminated veneer lumber according to EN 14374:2005-02 for non-load-bearing, load-bearing and stiffening elements*. Declaration of performance. Creuzburg, Germany: Pollmeier Furnierwerkstoffe GmbH, 2024.
- [3] EN 1995-2. *Eurocode 5: Design of timber structures – Part 2: Bridges*. Brussels, Belgium: European Committee for Standardization, 2004.
- [4] ETA-10/0241. *Leno Cross Laminated Timber – Züblin Timber GmbH*. European Technical Assessment. Berlin, Germany: Deutsches Institut für Bautechnik (DIBt), 2018.
- [5] ETA-19/0700. *SPIDER Connector and PILLAR Connector*. European Technical Assessment. Vienna, Austria: Austrian Institute of Construction Engineering (OIB), 2020.
- [6] P. Fast, B. Gafner, R. Jackson, and J. Li. “Case study: an 18 storey tall mass timber hybrid student residence at the University of British Columbia, Vancouver.” In: *Proceedings of the World Conference on Timber Engineering (WCTE 2016)*. Vienna, Austria: Vienna University of Technology, Austria, 2016. ISBN: 978-3-903039-00-1.
- [7] M. Kawrza, T. Furtmüller, C. Adam, and R. Maderebner. “Parameter identification for a point-supported cross laminated timber slab based on experimental and numerical modal analysis.” In: *European Journal of Wood and Wood Products* 79.2 (2020), pp. 317–333. DOI: 10.1007/s00107-020-01641-7.
- [8] K. A. Malo, R. B. Abrahamsen, and M. A. Bjertnæs. “Some structural design issues of the 14-storey timber framed building “Treet” in Norway.” In: *European Journal of Wood and Wood Products* 74.3 (2016), pp. 407–424. DOI: 10.1007/s00107-016-1022-5.
- [9] A. Münzer, K. Simon, C. Tapia, and S. Aicher. *Untersuchungen zu geklebten Rippen-Stützenkronen-Anschlüssen für die LCRL Stützen-Decker-Ausbildung*. Tech. rep. (in German). Stuttgart, Germany: Materials Testing Institute, University of Stuttgart, 2023.
- [10] M. Muster and A. Frangi. “Experimental analysis and structural modelling of the punching behaviour of continuous two-way CLT flat slabs.” In: *Engineering Structures* 205 (2020), p. 110046. DOI: 10.1016/j.engstruct.2019.110046.
- [11] L. Orozco, A. Krtschil, L. Skoury, J. Knippers, and A. Menges. “Arrangement of reinforcement in variable density timber slab systems for multi-story construction.” In: *International Journal of Architectural Computing* 20.4 (2022), pp. 707–727. DOI: 10.1177/14780771221135003.
- [12] T. Stieb, R. Maderebner, and P. Dietsch. “A Timber–Concrete–Composite Edge Connection for Two-Way Spanning Cross-Laminated Timber Slabs—Experimental Investigations and Analytical Approach.” In: *Buildings* 13.12 (2023), p. 3004. ISSN: 2075-5309. DOI: 10.3390/buildings13123004.
- [13] H. Svatoš-Ražnjević, L. Orozco, and A. Menges. “Advanced Timber Construction Industry: A Review of 350 Multi-Storey Timber Projects from 2000–2021.” In: *Buildings* 12.4 (2022), p. 404. DOI: 10.3390/buildings12040404.
- [14] C. Tapia, L. Stimpfle, and S. Aicher. “A scalable column-CLT-slab connection for open-plan high-rise timber buildings.” In: *Proceedings of the World Conference on Timber Engineering (WCTE 2021)*. Santiago, Chile: Centro UC de Innovación en Madera, 2021.

- [15] C. Tapia and S. Aicher. “A new concept for column-to-column connections for multi-storey timber buildings – Numerical and experimental investigations.” In: *Engineering Structures* 295 (2023), p. 116770. DOI: 10.1016/j.engstruct.2023.116770.
- [16] C. Tapia, M. Claus, and S. Aicher. “A finger-joint based edge connection for the weak direction of CLT plates.” In: *Construction and Building Materials* 340 (2022), p. 127645. DOI: 10.1016/j.conbuildmat.2022.127645.
- [17] C. Tapia, H. J. Wagner, S. Treml, A. Menges, and S. Aicher. “Point-Support Reinforcement for a Highly Efficient Timber Hollow Core Slab System.” In: *World Conference on Timber Engineering (WCTE 2023)*. Oslo, Norway, 2023. DOI: 10.52202/069179-0388.
- [18] S. Zöllig. “TS3 – A New Technology for Efficient Timber Structures.” In: *Current Trends in Civil & Structural Engineering* 4.4 (2020). ISSN: 2643-6876. DOI: 10.33552/ctcse.2020.04.000592.